Biomaterials Science

Accepted Manuscript

This article can be cited before page numbers have been issued, to do this please use: S. Y. Lee, E. Hong, J. Y. Jeong, J. Cho, J. Seo, H. Ko and H. Cho, *Biomater. Sci.*, 2019, DOI: 10.1039/C9BM00895K.

ROYAL SOCIETY OF CHEMISTRY

rsc.li/biomaterials-science

View Article Online
DOI: 10.1039/C9BM00895K

Esterase-sensitive cleavable histone deacetylase inhibitor-coupled hyaluronic acid nanoparticles for boosting anticancer activities against lung adenocarcinoma

Song Yi Lee[a,1], Eun-Hye Hong[b,1], Jae Young Jeong[a], Jaewon Cho[b], Ji-Hye Seo,[a] Hyun-Jeong Ko[b,*], Hyun-Jong Cho[a,**]

[a]College of Pharmacy, Kangwon National University, Chuncheon, Gangwon 24341, Republic of Korea.

[b]Laboratory of Microbiology and Immunology, College of Pharmacy, Kangwon National University, Chuncheon, Gangwon 24341, Republic of Korea.

[1]These authors equally contributed to this work.

[*] Corresponding author. Tel.: +82 33 250 6923; fax: +82 33 259 5631.

[**]Corresponding author. Tel.: +82 33 250 6916; fax: +82 33 259 5631.

E-mail addresses: hjko@kangwon.ac.kr (H.-J. Ko), hjcho@kangwon.ac.kr (H.-J. Cho).

View Article Online
DOI: 10.1039/C9BM00895K

ABSTRACT

4-Phenylbutyric acid (PBA)-installed hyaluronic acid (HA)-based nanoparticles (NPs) for amplifying anticancer potentials of curcumin (CUR) were developed for the therapy of lung cancer. PBA was introduced to HA backbone as a hydrophobic segment of nanoassembly structure and a histone deacetylase (HDAC) inhibitor for cancer therapy. PBA was released from HA-PBA conjugate (HAPBA) *via* an esterase-responsive cleavage of ester bond in cancer cells and it may affect the dissociation of NP's structure. CUR-entrapped HAPBA-based NPs with 265 nm hydrodynamic size, unimodal size distribution, negative zeta potential, and sustained drug release were fabricated. Co-treatment of PBA and CUR to A549 cells elevated antiproliferation efficiencies compared with CUR-treatment. CUR-loaded HAPBA NPs also exhibited significantly lower IC_{50} value compared with CUR and HAPBA10 + CUR groups ($p < 0.05$). Cy5.5-labeled HAPBA NPs containing CUR group displayed higher accumulation in tumor tissue and less distribution in liver and spleen compared with Cy5.5-injected group after intravenous injection in A549 tumor-bearing mouse model. Multiple dosing of CUR-loaded HAPBA NPs in A549 tumor-bearing mouse exhibited efficient tumor growth suppression and apoptosis inducing effects. CD44 receptor targeting and HDAC inhibiting HAPBA NPs can be used for boosting anticancer potentials of drug cargo for the therapy of CD44 receptor-expressed cancers.

Keywords: CD44 receptor, curcumin, hyaluronic acid, nanoparticle, 4-phenylbutyric acid

View Article Online
DOI: 10.1039/C9BM00895K

Introduction

A variety of tumor targeting strategies have been developed for increasing anticancer activities and reducing unwanted systemic toxicities.[1-4] Enhanced permeability and retention (EPR) effect, based on the leaky vasculatures and immature lymphatic systems of tumor region, has been introduced as a passive tumor targeting method.[5] However, incomplete tumor-targeting accuracy of EPR effect requires more elaborated targeting strategies. Active tumor targeting strategies based on the interactions between the ligand installed in nanocarriers and receptor expressed in cancer cells have been designed and many nanocarriers aimed at both passive and active tumor targeting have been developed.[6,7]

Among diverse pharmaceutical excipients for constructing nanostructures, biocompatible and biodegradable materials have been considered as ideal candidates. Hyaluronic acid (HA) is made of repeating disaccharides based on glucuronic acid and *N*-acetylglucosamine.[8] HA is synthesized by three different hyaluronan synthases (*i.e.,* HAS1, HAS2, and HAS3) and expelled through the plasma membrane to the cell surface or the extracellular matrix.[8] Then, it can be degraded by hyaluronidases.[8] Along with the biocompatibility and biodegradability of HA, its binding capability to CD44 and hyaluronan-mediated motility (RHAMM, CD168) receptors, overexpressed in many kinds of malignant tumor cells rather than normal cells, may provide tumor targetability during the development process of nanocarriers.[9-12] HA-based nanocarriers exhibited a remarkable tumor-selective drug delivery capability in various types of cancers.[9,11,13]

In our previous studies,[14-19] a couple of HA derivatives were synthesized and nanosystems based on those HA derivatives were prepared for tumor-targeted drug delivery after intravenous administration. Carboxylic, hydroxyl, and acetamido groups of HA can be used for its chemical modification.[20,21] Additive groups (*e.g.,* aminomethylphenylboronic acid, dopamine, folic acid, and polyethylene glycol) in HA derivatives can improve cellular

View Article Online
DOI: 10.1039/C9BM00895K

endocytosis, tumor penetration, and blood circulation during the drug delivery process to tumor region.[15,16,18,19]

4-Phenylbutyric acid (PBA) has been approved by US Food and Drug Administration for the treatment of urea cycle disorders and hyperammonemia.[22-24] PBA can act as a chemical chaperone by providing the restoration of proper conformation of proteins.[22] Of note, it can be used as an inhibitor of histone deacetylase (HDAC) and exhibited curative actions against malignant glioma, prostate cancer, colon cancer, and hepatocellular carcinoma.[22,25-28] Also, the hydrophobic property of PBA can contribute to construct a micellar structure for the delivery of poorly water-soluble drug.[29] In this study, PBA-modified HA (HAPBA) derivatives were synthesized and CUR-loaded HAPBA nanoparticles (NPs) were fabricated. PBA was joined as an inhibitor of HDAC for enhancing the anticancer potentials of incorporated curcumin (CUR) in lung adenocarcinoma as well as a hydrophobic segment for the preparation of nanoassembly structure. It is assumed that the incorporation of PBA and CUR into the HA-based single nanocarrier and their simultaneous delivery to tumor tissue may elevate the anticancer activities.

Experimental section

Materials

HA (molecular weight (MW): 4–8 kDa) was kindly supplied by SK Bioland Co., Ltd. (Cheonan, Korea). Tween 20 and Tween 80 was acquired from Tokyo Chemical Industry Co. Ltd. (Tokyo, Japan). CUR, deuterium oxide (D_2O), esterase, *N*-hydroxysuccinimide (NHS), *N*-(3-dimethylaminopropyl)-*N*'-ethylcarbodiimide hydrochloride (EDC), *N, N′*-dicyclohexylcarbodiimide (DCC), 4-(dimethylamino)pyridine (DMAP), hexadeuterodimethyl sulfoxide (DMSO-d_6), PBA, and polyethylene glycol 400 (PEG 400) were purchased from

View Article Online
DOI: 10.1039/C9BM00895K

Sigma–Aldrich (Saint Louis, MO, USA). Cy5.5-NH_2 (FCR-675 amine) was obtained from BioActs (DKC Corp., Incheon, Korea). Fetal bovine serum (FBS), penicillin-streptomycin, and RPMI 1640 (developed by Roswell Park Memorial Institute) were supplied by Gibco Life Technologies, Inc. (Grand Island, NY, USA).

Synthesis of HAPBA derivatives

HAPBA was synthesized *via* an esterification reaction between the carboxylic acid group of PBA and the hydroxyl group of HA. Several HAPBA derivatives with different feeding ratios between HA and PBA were synthesized in this study. For the synthesis of HAPBA02, HAPBA05, and HAPBA10, HA (250 mg) was dissolved in dimethyl sulfoxide (DMSO, 40 mL). The mixtures of PBA/DCC/DMAP (16.8 mg/20.7 mg/3.2 mg for HAPBA02, 42.0 mg/51.8 mg/8.0 mg for HAPBA05, and 84.0 mg/103.6 mg/16.0 mg for HAPBA10) were also dissolved in DMSO (10 mL). HA in DMSO and PBA/DCC/DMAP mixture in DMSO were blended and stirred for 24 h at room temperature. It was then dialyzed against the mixture of methanol and distilled water (DW) for 60 h with dialysis membrane (molecular weight cut-off (MWCO): 3.5 kDa). Freeze-dried resultant was washed with acetone at least thrice by centrifugation and resuspension processes. Purified resultant was lyophilized for further uses.

Characterization of HAPBA derivatives

The introduction of PBA to HA backbone was confirmed by proton nuclear magnetic resonance (^{1}H-NMR; Varian FT-500 MHz, Varian Inc., Palo Alto, CA, USA) spectroscopy analysis. For determining the content of PBA in HAPBA conjugates, the mixtures of HA and PBA (with different weight ratios between HA and PBA) were analyzed by ^{1}H-NMR spectroscopy. Samples were dissolved in the mixture of D_2O and DMSO-d_6 (1:1, v/v) for ^{1}H-NMR analysis. According to ^{1}H-NMR data, a regression line of integration ratio of peaks

View Article Online
DOI: 10.1039/C9BM00895K

(7.1-7.3 ppm/1.8-1.9 ppm) to weight ratio (PBA/HA) was constructed. By using this regression line, the contents of PBA in HAPBA02, HAPBA05, and HAPBA10 were calculated.

The particle size, size distribution, and surface charge of dispersion of synthesized HAPBA conjugates were measured by dynamic light scattering (DLS) and laser Doppler methods (ELS-Z1000; Otsuka Electronics, Tokyo, Japan).[30] HAPBA02, HAPBA05, and HAPBA10 were dispersed in DW at 10 mg/mL for the analysis of particle properties.

Synthesis of HAPBA10 was further identified with Fourier-transform infrared (FT-IR) spectroscopic analysis (Frontier™ FT-IR spectrometer; PerkinElmer Inc., Buckinghamshire, UK). Attenuated total reflectance (ATR) mode was selected for obtaining FT-IR data of HA, PBA, and HAPBA10. Wavenumber (cm^{-1})-dependent transmittance (%) of each sample was scanned.

Thermogravimetric (TGA) analysis was performed with a thermal analysis system (SDT Q600, TA instruments, New Castle, DE, USA). Weight change profiles according to the temperature of HA, PBA, and HAPBA10 were measured.

Release of PBA from HAPBA10 in the presence or absence of esterase was measured after incubating 24, 48, and 72 h. HAPBA10 was dispersed in phosphate buffered saline (PBS, pH 7.4) at 10 mg/mL and esterase was added at 0.5 mg/mL. Aliquots (1 mL) of HAPBA10 or HAPBA10+esterase dispersion were incubated for 24, 48, and 72 at 37°C. At each time point, the sample was filtered through syringe filter membrane (pore size: 0.2 μm) prior to high-performance liquid chromatography (HPLC) analysis of PBA. HPLC system (1260 Infinity II, Agilent Technologies, Santa Clara, CA, USA) equipped with autosampler (1260 Vialsampler), pump (1260 Quat Pump VL), UV/Vis detector (1260 VWD), and a reverse phase C18 column (Kinetex, 250 mm × 4.6 mm, 5 μm; Phenomenex, Torrance, CA, USA) was used for the quantitative analysis of PBA. The mobile phase was composed of the

View Article Online
DOI: 10.1039/C9BM00895K

mixture of 20 mM KH_2PO_4 (pH 3.1 adjusted with H_3PO_4) and methanol (40:60, v/v). The wavelength, column temperature, flow rate of mobile phase, and injection volume were 265 nm, 40°C, 1 mL/min, and 20 μL. Linearity was established in 1–100 μg/mL concentration range with developed 4PBA analysis method.

Preparation and particle characterization of CUR-entrapped NPs

CUR-loaded HAPBA NPs were prepared by using a dialysis method.[16,31] CUR (5 mg) was dissolved in 75% (v/v) DMSO (8 mL) and HAPBA conjugate (75 mg) was added to that solution. That resultant was put into the dialysis bag (MWCO: 3.5 kDa) and it was dialyzed against DW for 8 h. It was lyophilized for further uses.

Particle properties (mean diameter, polydispersity index, and zeta potential) of fabricated HAPBA02/CUR NPs, HAPBA05/CUR NPs, and HAPBA10/CUR NPs were investigated by DLS and laser Doppler method (ELS-Z1000; Otsuka Electronics, Tokyo, Japan).[30] Prior to the analysis of particle properties, lyophilized HAPBA/CUR composites were dispersed in DW. The encapsulation efficiency of CUR in NPs was determined by HPLC system.[31,32] A reverse phase C18 column (Gemini, 250 mm × 4.6 mm, 5 μm; Phenomenex, Torrance, CA, USA) installed with a guard column (SecurityGuard Guard Cartridge kit, Phenomenex, Torrance, CA, USA) was connected to the HPLC system composed of a pump (PU-2089 Plus; Jasco, Tokyo, Japan), an automatic injector (AS-2050 Plus), and an UV/Vis detector (UV-1575) as reported.[31,23] CUR-incorporated NPs were dissolved in DMSO for measuring its encapsulation efficiency in NPs. The mobile phase was based on the mixture of acetonitrile, tetrahydrofuran, and water (35:20:45, v/v/v). The flow rate was maintained at 1 mL/min and the injection volume was set as 20 μL. The absorbance of each sample was detected at 425 nm.

The particle shape of HAPBA10/CUR NPs was observed by transmission electron

View Article Online
DOI: 10.1039/C9BM00895K

microscopy (TEM). Lyophilized NPs were dispersed in DW and stained with 2% (w/v) phosphotungstic acid. Washed specimen was put onto the copper grids with films and air-dried for TEM (JEM 1010; JEOL, Tokyo, Japan) analysis.[19]

Particle stability of HAPBA10/CUR NPs was assessed after incubation in PBS (pH 7.4). Hydrodynamic size of HAPBA10/CUR NPs in PBS (at 2.5 mg/mL) was measured by DLS method at 0, 2, 4, and 24 h.

CUR release pattern from HAPBA10/CUR NPs was tested after incubation in PBS (pH 7.4 and 5.5).[31] Dispersion (0.45 mL) of HAPBA10/CUR NPs including 300 μg CUR was loaded into the dialysis tubing with 12–14 kDa MWCO (Viscase Companies, Inc., Lombard, IL, USA). It was immersed in PBS (pH 7.4, 30 mL) including 0.1% Tween 80 and incubated at 50 rpm and 37°C. At determined times (3, 6, 24, 48, 72, 96, and 120 h), aliquots of release media (0.2 mL) were withdrawn. CUR concentrations in collected release media sample were quantitatively analyzed by described HPLC method.

Cellular internalization and localization tests

For tracing *in vitro* cellular movement of fabricated NPs by fluorescence detection, Cy5.5 was labeled to the synthesized HAPBA10 conjugate. EDC/NHS-coupled amide bond formation strategy was introduced to synthesize Cy5.5-HAPBA10 in this study. HAPBA10 (96 mg) was solubilized in DMSO (18 mL) and pH 4 was attained by adding 1N HCl to that solution. EDC (1.15 mg) and NHS (0.69 mg) dissolved in DMSO (1 mL) was then added to that solution and it was stirred for 15 min. After adjusting with 1N NaOH for neutralization, Cy5.5-NH_2 (2.4 mg) dissolved in DMSO (1 mL) was put into that mixture and stirred for 24 h at room temperature. It was dialyzed against DW for 2 days with dialysis membrane (MWCO: 3.5 kDa) and freeze-dried for further uses.

Cellular accumulation efficiency of Cy5.5-conjugated HAPBA10/CUR NPs in A549

View Article Online
DOI: 10.1039/C9BM00895K

cells (Korean Cell Line Bank, Seoul, Korea) was assessed by flow cytometry. A549 cells were cultured with RPMI 1640 containing FBS (10%) and penicillin-streptomycin. A549 cells were seeded onto 6-well plate at a density of 4.0×10^5 cells per well and incubated for 1 day. Cy5.5 solution or Cy5.5-HAPBA10/CUR NPs dispersion (containing 25 μg/mL Cy5.5) was applied to the cells and incubated for 1, 2, and 6 h. In addition, to verify CD44 receptor-assisted endocytosis of HA nanocarriers, HA oligomer (2 mg/mL) was pre-treated for 30 min and co-treated during the incubation time (1 and 2 h) with Cy5.5-HAPBA10/CUR NPs. After rinsing with PBS, cells were harvested and resuspended in FBS (2%, v/v) solution. Fluorescence intensity-dependent cell count was measured by a FACSCalibur Fluorescence-activated Cell Sorter (FACS™) installed with CELLQuest software (Becton Dickinson Biosciences, San Jose, CA, USA).

Cellular localization of fabricated NPs was monitored by confocal laser scanning microscopy (CLSM) analysis. A549 cells (1.0×10^5 cells per well) were seeded in culture slides (1.7 cm^2 surface area per well; BD Falcon, Bedford, MA, USA) and incubated for 1 day. Cy5.5 solution or Cy5.5-HAPBA10/CUR NPs dispersion (containing 25 μg/mL Cy5.5) was applied to the cells and incubated for 1, 2, and 6 h. For staining lysosome, Cy5.5 and Cy5.5-HAPBA10 NPs groups (at 10 μg/mL Cy5.5) were incubated for 3 h with LysoTracker Green DND-26 (Invitrogen, Carlsbad, CA, USA) (at 100 nM and for 1 h). Cells were rinsed with PBS (pH 7.4) and they were fixed in formaldehyde solution for staining. 4',6-Diamidino-2-phenylindole (DAPI) included VECTASHIELD mounting medium (H-1200; Vector Laboratories, Inc., Burlingame, CA, USA) was used for staining nuclei and preventing fluorescence quenching. Cellular fluorescence signals were then monitored by CLSM (LSM 880, Carl-Zeiss, Thornwood, NY, USA).

In vitro anticancer activity tests

View Article Online
DOI: 10.1039/C9BM00895K

In vitro antiproliferation potential of developed CUR-loaded NPs was tested in A549 cells by MTS-based assay. A549 cells (2.0×10^3 cells per well) were seeded in 96-well plate and incubated for 1 day. The combination effect of PBA and CUR on the antiproliferation efficacy was evaluated by comparison between PBA and PBA + CUR (10 μg/mL) groups. The role of HAPBA10 in the toxicity of CUR was assessed by applying HA, HAPBA10, and HAPBA10 + CUR (10 μg/mL) groups in A549 cells. The antiproliferation efficiency of CUR-loaded NPs was tested after incubating with CUR, HAPBA10 + CUR, and HAPBA10/CUR NPs in A549 cells. Cells were incubated with each sample for 72 h and they were treated with MTS-based CellTiter 96® AQ_{ueous} One Solution Cell Proliferation Assay Reagent (Promega Corp., Fitchburg, WI, USA). The absorbance of each specimen was read at 490 nm with UV/Vis spectrometer (EMax Precision Microplate Reader; Molecular Devices, Sunnyvale, CA, USA).[30] Cell viability was calculated by comparing the absorbance value of test group with that of control (no treatment) group.

Apoptosis induction potentials of CUR-entrapped NPs were tested in A549 cells. A549 cells (at a density of 1.0×10^5 cells per well) were seeded in 6-well plates and they were incubated for 1 day. HAPBA10 (corresponding to 10 μg/mL CUR), CUR (10 μg/mL), HAPBA10/CUR NPs (corresponding to 10 μg/mL CUR), PBA (500 μg/mL), and PBA (500 μg/mL) + CUR (10 μg/mL) were applied to the cells and they were incubated for 24 and 48 h. Those cells were rinsed with PBS (pH 7.4) after removing each sample. Cells were then harvested and resuspended in the reaction buffer of FITC Annexin V Apoptosis Detection Kit (BD Pharmingen, BD Biosciences, San Jose, CA, USA).[30] Corrected cellular fluorescence intensity values of Annexin V-FITC and PI were measured by FACSCalibur fluorescence-activated cell sorter (FACS™).

Bio-distribution study

View Article Online
DOI: 10.1039/C9BM00895K

Bio-distribution of CUR-entrapped NPs in tumor-bearing mouse model was visualized by near-infrared fluorescence (NIRF) imaging. For NIRF detection, Cy5.5 was attached to HAPBA10 conjugate for the preparation of CUR-included NPs. The content of Cy5.5 in Cy5.5-HAPBA10/CUR NPs was determined based on the absorbance values at 680 nm.

A549 tumor-bearing mouse model was prepared with female BALB/c nude mice (~20 g average body weight, 5 weeks old; Orient Bio Inc., Seongnam, Korea).[33] The experimental protocols were approved by the Animal Care and Use Committee of the Kangwon National University. Animal studies were carried out according to the National Institutes of Health guide for the care and use of Laboratory animals (NIH Publications No. 8023, revised 1978). Suspension of A549 cells (2.0×10^6 cells in 0.1 mL) was injected into the dorsal side of the mice. The tumor volume (V, mm^3) was obtained as follows: V = (1/2) × longest diameter × (shortest diameter)^2. After obtaining 150–200 mm^3 tumor volume, free Cy5.5 solution or Cy5.5-HAPBA10/CUR NP dispersion, containing 100 μg/kg dose of Cy5.5, was injected to the mouse intravenously. Images of whole body were scanned by Spectral Lago X (Spectral Instruments Imaging; Tucsan, AZ, USA) equipped with Cy5.5 filter (excitation: 640 nm; emission: 710 nm) at 0 (pre), 4, and 24 h postinjection. Quantitative analysis of NIRF intensity was conducted with AMIView software (ver. 1.7.01). Heart, lungs, liver, spleen, kidneys, and tumor were excised from the mouse at 24 h postinjection and *ex vivo* NIRF image was obtained. Total effective intensity of region of interest (ROI) was calculated by multiplying mean effective intensity with effective area (cm^2). Half-life of Cy5.5-HAPBA10/CUR NPs was also estimated by time-dependent NIRF signals in normal ICR mouse (8 weeks old; Orient Bio Inc., Seongnam, Korea) after intravenous injection. Dispersion of Cy5.5-HAPBA10/CUR NPs (at 100 μg/kg dose of Cy5.5) was injected to the mouse intravenously and the whole-body scanned images were taken at day 0 (pre and after-injection), 1, 2, 3, 4, 7, 10, and 14.

View Article Online
DOI: 10.1039/C9BM00895K

In vivo anticancer potential studies

In vivo antitumor efficacies of CUR-contained NPs were evaluated in A549 tumor-bearing murine models with slightly modified reported protocol.[33] A549 tumor-implanted mice were developed as presented in the previous section. BALB/c nude mice (female, ~20 g average body weight, 5 weeks old) were used for the preparation of A549 tumor-bearing mouse model in this study. After reaching approximately 150 mm^3 tumor volume, those mice were randomly divided into four groups. CUR solution (1 mg/mL) was prepared by solubilizing CUR in 37.5% (w/w) PEG 400 solution in DW.[31] HAPBA10 dispersion, CUR solution, or HAPBA10/CUR NPs dispersion (at 5 mg/kg dose of CUR and 5 mL/kg injection volume) was injected intravenously to the tumor-bearing mouse model on day 4, 9, 12, 15, 18 and 22. Body weight was also measured at the same time points. On day 36, tumor mass was excised and it was fixed in formaldehyde (4%, v/v) solution for histological staining. Fixed tumor tissues were cut into the slices and they were deparaffinized and hydrated with ethanol. Those tumor tissues were then stained with hematoxylin and eosin (H&E) reagent and consecutively with terminal deoxynucleotidyl transferase dUTP nick end labeling (TUNEL) assay reagent.[34] For TUNEL assay, 3,3'-diaminobenzidine (DAB) was used for color development in tumor tissues. The expression levels of apoptosis-related markers (caspase-3 and poly (ADP-ribose) polymerase (PARP)/cleaved PARP (c-PARP)) in excised tumor tissue were quantitatively analyzed by western blotting. Tumor tissue samples were prepared by sonication in lysis buffer (iNtRON, Seongnam, Korea). Equal amounts of sample lysates were heated at 100°C and loaded for sodium dodecyl sulfate-polyacrylamide gel electrophoresis (SDS-PAGE). Proteins were transferred to polyvinylidene difluoride (PVDF) membranes (Millipore, Billerica, MA, USA) and then blocked with 5% milk in Tris-buffered saline and 0.1% Tween 20. The membranes were incubated 2 h with primary Abs against

View Article Online
DOI: 10.1039/C9BM00895K

PARP/c-PARP, caspase-3, and β-actin (Cell Signaling Technology, Inc., Danvers, MA, USA), and goat-anti-rabbit Abs conjugated with horseradish peroxidase (HRP) detect proteins (Cell Signaling Technology, Inc., Danvers, MA, USA). Enhanced chemiluminescence (ECL) method with femtoLUCENT™ PLUS-HRP (G-biosciences, St. Louis, MO, USA) was used for the detection of proteins.

Data analyses

Data were statistically analyzed with a two-tailed *t*-test and analysis of variance (ANOVA). Each experiment was repeated at least thrice. Data are shown as the mean ± standard deviation (SD).

Results

Synthesis and characterization of HAPBA

HAPBA NPs containing CUR were designed based on the self-assembly nanostructure strategy (Fig. 1). HA grafted with different feeding ratios of PBA was synthesized by DCC/DMAP-mediated esterification reaction (Fig. 2). Peak 1 at 1.8-1.9 ppm and peak 2 and 3 at 7.1-7.3 ppm indicate *N*-acetyl group of HA and phenyl ring of PBA, respectively. HAPBA02, HAPBA05, and HAPBA10 were synthesized with different weight ratios of PBA, DCC, and DMAP to HA. The mean contents of PBA in HAPBA02, HAPBA05, and HAPBA10, analyzed by ^{1}H-NMR spectroscopic method, were 0.14%, 0.21%, and 0.56%, respectively (Fig. 2 and Fig. S1).

Prior to CUR loading in the HAPBA NPs, particle properties of blank HAPBA dispersion in DW were evaluated (Table 1). The hydrodynamic size values of HAPBA02, HAPBA05, and HAPBA10-based particles were 900 nm, 977 nm, and 721 nm, respectively.

View Article Online
DOI: 10.1039/C9BM00895K

All those samples exhibited negative zeta potential values.

Attachment of PBA to HA was identified by FT-IR analysis (Fig. S2A). Although C=O stretching band (1728 cm^{-1}) of free COOH group and C=O stretching band (1630 cm^{-1}) of COO^- group were shown in the spectrum of HA, C=O stretching band was present at 1652 cm^{-1} in HAPBA10 group.[35] C–O stretching bands (C–O–C) in HA group (*i.e.,* 1021 cm^{-1}) were also observed in HAPBA10 group (*i.e.,* 1033 cm^{-1}).[35] C–H stretching bands in PBA group (*i.e.,* 2927 cm^{-1}) were also shown in HAPBA10 group (*i.e.,* 2930 cm^{-1}). TGA profiles of HA, PBA, and HAPBA10 were also acquired for verifying the synthesis of HAPBA10 in this study (Fig. S2B). Weight loss percentages of HA and HAPBA10 at 150°C, probably due to the elimination of water, were 12.8% and 12.9%, respectively.[36] Those of HA and HAPBA10 at 300°C were 54.3% and 58.6%, respectively, and they exhibited different TGA profiles.

PBA release from HAPBA10 with or without esterase was measured according to the incubation time (Fig. 2C). In both groups (HAPBA10 and HAPBA10+esterase), higher released amounts of PBA were shown in longer incubation period. At 24 h sample of HAPBA10, the PBA concentration was under the limit of detection. After 72 h incubation, the released amounts of PBA from HAPBA10 and HAPBA10+esterase groups were 2.6% and 41.5%, respectively.

Preparation and characterization of CUR-entrapped NPs

CUR, as a poorly water-soluble drug, was entrapped in the internal hydrophobic cavity of HAPBA-based nanostructure by dialysis method in this study. Hydrodynamic size values of HAPBA02/CUR NPs, HAPBA05/CUR NPs, and HAPBA10/CUR NPs were 597 nm, 549 nm, and 265 nm, respectively (Table 1). Interestingly, HAPBA10/CUR NPs displayed suitable particle size for the EPR effect, unimodal size distribution, and negative zeta

View Article Online
DOI: 10.1039/C9BM00895K

potential value (Table 1 and Fig. 3A). Round shape of HAPBA10/CUR NPs was also observed by TEM imaging (Fig. 3B). The initial hydrodynamic size of HAPBA10/CUR NPs was maintained even after 24 h incubation in PBS (pH 7.4) (Fig. 3C). Due to the higher stability of CUR at acidic pH (pH 5.5) rather than normal pH (pH 7.4), higher released amount of CUR was shown in the terminal period of release test at pH 5.5 (Fig. 3D). Sustained drug release profile without a marked initial burst release was also observed in HAPBA10/CUR NPs group in this study (Fig. 3D).

Cellular internalization and distribution

Cellular internalization efficiency of prepared NPs in A549 cells was assessed by flow cytometry (Fig. 4A). For fluorescence detection of NPs, Cy5.5 was chemically attached to HA backbone. Cy5.5 group exhibited declining pattern in fluorescence intensity, indicating the decrease of cellular accumulation, while Cy5.5-HAPBA10/CUR NPs group displayed increasing pattern for 6 h. Notably, the mean fluorescence intensity of Cy5.5-HAPBA10/CUR NPs group was 2.4-fold higher than that of Cy5.5 group at 6 h ($p < 0.05$). With the treatment of HA oligomer, the cellular accumulation efficiency of Cy5.5-HAPBA10/CUR NPs in A549 cells was reduced to 70% and 77% at 1 and 2 h incubation, respectively (Fig. S3). Cellular distribution of NPs in A549 cells was observed by CLSM imaging (Fig. 4B). Red fluorescence signals of Cy5.5 indicate the cellular localization of Cy5.5-modified NPs. As shown in Fig. 4A, increasing profile in red fluorescence intensity was observed in Cy5.5-HAPBA10/CUR NPs group during 6 h. Although green fluorescence of Lysotracker seemed to be interfered with Cy5.5, HAPBA10 NPs were also distributed in lysosome (Fig. S4).

***In vitro* anticancer potentials**

View Article Online
DOI: 10.1039/C9BM00895K

The combination effect of PBA and CUR on the improvement of anticancer potentials was tested by antiproliferation assay in A549 cells (Fig. 5A). Compared to PBA group, PBA + CUR (10 μg/mL) group exhibited higher cytotoxic potentials in 10–1000 μg/mL of PBA concentration range ($p < 0.05$). The combinatorial effect of HAPBA10 and CUR in anticancer activity was also investigated by HAPBA10 concentration-dependent cell viability test (Fig. 5B). While HA did not show a significant cytotoxicity at 10–2000 μg/mL of HA concentration range, HAPBA10 exhibited antiproliferation potentials at 2000 μg/mL of HAPBA10 concentration. After co-incubation with CUR (10 μg/mL), cell viability values were lower than those of HAPBA10 group at 10–1000 μg/mL of HAPBA10 concentration range ($p < 0.05$). The antiproliferation efficacy of HAPBA10/CUR NPs was evaluated in A549 cells by comparison with CUR and HAPBA10 + CUR groups (Fig. 5C). IC_{50} values of CUR, HAPBA10 + CUR, and HAPBA10/CUR NPs groups were 18.2 ± 0.1, 15.9 ± 0.5, and 13.0 ± 0.8 μg/mL, respectively (Fig. 5C). Cytotoxic potential of HAPBA10/CUR NPs group was significantly higher than those of CUR and HAPBA10 + CUR groups ($p < 0.05$).

Apoptosis inducing effects of HAPBA10/CUR NPs were assessed by Annexin V and PI-based assay in A549 cells (Fig. 6). The sum of population percentage in lower right (LR) and upper right (UR) panels has been used for the indication of apoptotic population. HAPBA10 or PBA treatment did not induce a significant apoptosis in A549 cells compared to control (no treatment) group. The apoptotic population percentage of PBA + CUR group was slightly higher than that of CUR group after 24 and 48 h incubation. The sum of population percentage in (LR + UR) panel of HAPBA10/CUR NPs group was also higher than those of the other groups at 24 and 48 h incubation groups.

In vivo and *ex vivo* NIRF imaging

Tumor targeting capability and bio-distribution pattern of HAPBA/CUR NPs in A549 tumor-

View Article Online
DOI: 10.1039/C9BM00895K

bearing mouse model were investigated by an optical imaging (Fig. 7). Compared with Cy5.5-injection group, higher NIRF intensity in tumor tissue (presented as an intensity of ROI) was presented in Cy5.5-HAPBA10/CUR NPs group at 4 and 24 h ($p < 0.05$) (Fig. 7A and 7B). Biodistribution of injected NPs was further evaluated by *ex vivo* NIRF imaging. As shown in Fig. 7C and 7D, fluorescence intensity in (liver + spleen) of Cy5.5-HAPBA10/CUR NPs group was significantly lower than that of Cy5.5 group ($p < 0.05$). Fluorescence intensity in dissected tumor tissue of Cy5.5-HAPBA10/CUR NPs group was 3.9-fold higher than that of Cy5.5 group ($p < 0.05$) (Fig. 7D). The fluorescence intensity ratios of tumor to (liver + spleen) in Cy5.5 and Cy5.5-HAPBA10/CUR NPs groups were 0.03 and 0.25, respectively. Cy5.5-HAPBA10/CUR NPs were intravenously injected to normal ICR mouse and time-dependent NIRF signals were quantitatively determined (Fig. S5). Estimated half-life of Cy5.5-HAPBA10/CUR NPs was approximately 7 days in normal ICR mouse.

In vivo anticancer activities

In vivo anticancer potentials of HAPBA10/CUR NPs were verified in A549 tumor-bearing mouse models (Fig. 8). HAPBA10/CUR NPs-injection group exhibited significant tumor growth suppression effects rather than control, HAPBA10, and CUR groups on day 32 and 36 ($p < 0.05$) (Fig. 8A). There was no significant difference among all experimental groups (control, HAPBA10, CUR, and HAPBA10/CUR NPs) in body weight on day 36 (Fig. 8B). According to H&E staining images (Fig. 8C), multiple injection of HAPBA10/CUR NPs did not induce significant histological changes in heart, liver, lung, kidney, and spleen compared with control group. Remarkably, higher apoptotic portion (shown as a brown color) was presented in HAPBA10/CUR NPs group rather than the other groups as shown in TUNEL assay data (Fig. 8C). Apoptosis-related protein expression levels in excised tumor tissues were also assessed by western blotting assay (Fig. 8D and Fig. S6). Relative expression levels

View Article Online
DOI: 10.1039/C9BM00895K

of caspase-3 and c-PARP in HAPBA10/CUR NPs group were significantly higher than those of the other groups (control, HAPBA10, and CUR groups) ($p < 0.05$).

Discussion

PBA has been introduced as a hydrophobic moiety to hydrophilic HA backbone to constitute self-assembled nanostructure in the aqueous environment. PBA also has been regarded as one of chemical chaperones, which can correct protein folding and prevent its aggregation and degradation.[37] As shown in "butylate paradox", it has cytotoxic effects in cancer cells in contrast to cytoprotection properties in normal cells.[22,38] Also, it can act as an inhibitor of HDAC and exhibit anticancer potentials in malignant tumor cells and pharmacological efficacies against diabetes mellitus and cardiovascular diseases.[39] HDAC inhibition may lead to the improvement of histone acetylation, DNA relaxation, and transcriptional activity in cancer cells.[22] These regulation may further produce improved apoptosis, induction of differentiation, enhanced antiproliferation, reduced metastatic activities, downregulated tumor angiogenesis, increased sensitivity in chemotherapy, and improved autophagy in cancer therapy.[22] Although high content of PBA in HAPBA may be beneficial to anticancer approaches, it may also increase hydrophobicity of synthesized HAPBA conjugate which can disturb the formation of nano-sized particles in the aqueous environment. Considering the lowest hydrodynamic size of blank HAPBA10 conjugate dispersion (Table 1), it was selected as a final candidate of an amphiphilic conjugate for the fabrication of CUR-incorporated NPs in this study. The presence of proton chemical shifts at 7.1-7.3 ppm (peak 2 and 3) indicates the successful introduction of PBA to HA backbone (Fig. 2). In addition, the increase in PBA contents along with the increment in feeding ratios of PBA to HA also implies the synthesis of HAPBA conjugates (Fig. 2). Negative zeta potential values of blank HAPBA conjugate dispersion seem to be based on the exposure of carboxylic acid groups in the outer HA shell

View Article Online
DOI: 10.1039/C9BM00895K

of NPs. As HA and PBA include carboxylic acid groups, it is not easy to identify the ester bond formation in HAPBA10 conjugate by FT-IR analysis (Fig. S2A). However, C–O and C=O stretching bands in HA were present at different wavenumber compared with those of HAPBA10 and C–H stretching bands of PBA were also included in the spectrum of HAPBA10. These evidences imply the proper conjugation of HAPBA10. In TGA analysis (Fig. S2B), HAPBA10 group exhibited slightly different TGA profile compared to HA group. The chemical conjugation of PBA to HA seems to alter its thermal properties. Enzyme-responsive PBA release from HAPBA10 was tested in the presence or absence of esterase (Fig. 2C). Esterase-sensitive ester bond uncoupling approach has been used in the design of nanosystems for on demand drug release in the cancer cells.[40,41] Esterase in the cellular space of cancer cells may cleavage the ester linkage of HAPBA10 after its endocytosis. PBA was efficiently released from HAPBA10 in the presence of esterase, compared to the group without esterase. Detached PBA after endocytosis in cancer cells may assist the antitumor efficacies of CUR in this study.

With the anticancer potentials of PBA installed in NPs, CUR was introduced in the internal part of NPs for the therapy of lung adenocarcinoma in this study. Due to the poor water solubility of CUR, it should be formulated for intravenous injection. Compared with the hydrodynamic size (> 500 nm) of HAPBA02/CUR NPs and HAPBA05/CUR NPs, the mean diameter (265 nm) of HAPBA10/CUR NPs seems to be more appropriate for EPR effect-related passive tumor targeting.[5,6,42,43] Thus, HAPBA10/CUR NPs group was selected for further development processes of intravenous injection formulation in this study. It also presented unimodal size distribution, spherical shape, and negative surface charge as shown in Table 1 and Fig. 3. Particle size reduction after CUR loading may be explained by the interactions between hydrophobic CUR molecules and hydrophobic domain (*i.e.,* PBA) of internal cavity of NPs. The absence of aggregation of NPs after incubating in PBS indicates

View Article Online
DOI: 10.1039/C9BM00895K

the negligible influences of pharmaceutical salts on the particle stability (Fig. 3C). It may further guarantee the maintenance of particle stability in the biological fluids after intravenous administration and contribute to the safety for clinical application. Sustained drug release from fabricated HAPBA10/CUR NPs may also reduce dosing frequency and improve patient compliance in intravenous injection (Fig. 3D). Higher stability of CUR itself at acidic pH (pH 5.5) rather than normal pH (pH 7.4) may be lead to higher CUR accumulation in endosomes and lysosomes of cancer cells (pH 5.5) rather than normal tissues and organs (pH 7.4).[32] Cleavage of ester bond in HAPBA10 by esterase and subsequent PBA release may disrupt the self-assembled structure of NPs. CUR release can be related to the dissociation of NP's structure.

Cellular internalization efficiency and cellular fate of NPs were tested by flow cytometry and CLSM analysis, respectively (Fig. 4). For 6 h of incubation, free Cy5.5 and Cy5.5-labeled NPs groups displayed declining and inclining patterns, respectively, in fluorescence intensity. It seems that free Cy5.5 and Cy5.5-HAPBA10/CUR NPs may be transported *via* simple diffusion and receptor-mediate endocytosis, respectively. In particular, HA-based nanocarriers exhibited CD44 receptor-mediated endocytosis in cancer cells in our previous studies.[14-19] As reported previously,[14-19] HA treatment with Cy5.5-HAPBA10/CUR NPs reduced the cellular accumulation efficiency significantly and it means the contribution of HA-CD44 receptor interaction for the endocytosis of HA-based nanaocarriers (Fig. S3). In addition, fabricated HAPBA10-based NPs seemed to be distributed in the cytoplasm including lysosome and it may lead to the cleavage of HAPBA conjugate by cellular esterase (Fig. S4). Selective uptake into the cancer cells may improve the anticancer potentials of drug cargo in NPs after intravenous administration without severe unwanted toxicities to normal organs and tissues.

The contribution of incorporation of both PBA and CUR into the single nanocarrier to

View Article Online
DOI: 10.1039/C9BM00895K

anticancer activities was tested in A549 cells (Fig. 5). HAPBA conjugate might be degraded into HA and PBA by esterase in the lysosomal compartment (Fig. 2C) and CUR can be also released from HAPBA NPs.[44] Co-incubation of CUR (10 μg/mL) with PBA amplified cytotoxicity obviously in A549 cells compared with PBA group (Fig. 5A). Considering the cell viability (approximately 80%) at 10 μg/mL CUR (Fig. 5C), simultaneous treatment of PBA and CUR seems to provide synergistic antiproliferation capabilities in A549 cells. It implies that PBA included in NPs can elevate the anticancer activities of CUR in A549 cells. The contribution of HAPBA10 to the anticancer activities of CUR was also tested in A549 cells (Fig. 5B). Lower cell viability values of HAPBA10 + CUR (10 μg/mL) group, rather than HAPBA10 group, at 10–1000 μg/mL HAPBA10 concentration range may identify the role of HAPBA10 for elevating antiproliferation potentials. It is expected that the entrapment of both HAPBA10 and CUR into the single nanocarrier can enhance their anticancer activities in A549 cells. Antiproliferation potentials were finally evaluated by comparing the cell viability values of CUR, HAPBA10 + CUR, and HAPBA10/CUR NPs groups (Fig. 5C). HAPBA10/CUR NPs group displayed the lowest IC_{50} value and it can suggest the usefulness of PBA and CUR entrapped NPs for cancer therapy. Along with HDAC inhibition properties of PBA, CUR also possesses anti-oxidant and anticancer efficacies. Diverse signaling pathways, such as NF-κB, STAT3, Sp-1, and housekeeping genes, were reported to be involved in the anticancer activities of CUR.[45] Improved apoptosis, induction of differentiation, enhanced antiproliferation, reduced metastatic activities, downregulated tumor angiogenesis, increased sensitivity in chemotherapy, and improved autophagy of PBA can produce the elevation of anticancer potentials of HAPBA10/CUR NPs in this study.

Combinatory effect of CUR and PBA for inducing apoptosis in cancer cells was investigated by Annexin V and PI-based assay (Fig. 6). PBA has been known as one of inhibitors of HDAC.[46] Most of them can inhibit HDAC enzymes as Zn^{2+}-dependent manner

View Article Online
DOI: 10.1039/C9BM00895K

and their anticancer potentials were systemically demonstrated in cell culture and animal models.[22] Although PBA treatment did not show elevated apoptosis inducing effects in tested PBA concentration, its combination with CUR exhibited an obvious improvement in apoptosis induction in A549 cells. HDAC inhibitory properties of PBA included in HAPBA10 seem to provide the enhancement of apoptosis when it was used with CUR in this study. Release of PBA by esterase-sensitive cleavage of ester bond and CUR by dissociation of NPs can provide these apoptotic potentials. Highest apoptotic percentage of HAPBA10/CUR NPs group also supports the assistance of PBA for exerting therapeutic potentials of CUR.

Tumor targeting efficiency and *in vivo* fate of injected CUR-loaded NPs were tested in A549 tumor-bearing mouse model (Fig. 7). Passive tumor targeting (related to an EPR effect) and active tumor targeting (based on HA-CD44 receptor interactions) strategies of amphiphilic HA derivative-based NPs were already demonstrated in our previous reports.[14-19] According to whole body scanned images (Fig. 7A and 7B), considerable amounts of Cy5.5-conjugated NPs were still retained in tumor region compared with Cy5.5 group at 24 h ($p < 0.05$). Polymeric NPs can be considered as foreign materials thus they are used to be accumulated in reticuloendothelial system (*i.e.,* liver and spleen). Considering the fluorescence intensity ratios of tumor/(liver + spleen) in Cy5.5 (0.03) and Cy5.5-HAPBA10/CUR NPs (0.25), developed NPs seem to be less distributed in liver and spleen and be efficiently moved to tumor tissue compared with Cy5.5 group (Fig. 7C and 7D). These findings imply the efficient tumor-targeted delivery of fabricated CUR-loaded NPs and less distribution in normal tissues and organs. They may be lead to selective tumor growth inhibition without severe toxicities to normal tissues and organs. Half-life of designed Cy5.5-HAPBA10/CUR NPs was approximately 7 days in normal ICR mouse after intravenous injection according to the dorsal-side scanned NIRF images (Fig. S5). Fabricated NPs seem

View Article Online
DOI: 10.1039/C9BM00895K

to be sufficiently circulated in the blood stream after intravenous injection and it may contribute to reduce dosing frequency.

Anticancer activities of PBA-installed NPs including CUR were demonstrated in A549 tumor-xenografted murine model (Fig. 8 and Fig. S6). HAPBA10/CUR NPs group displayed the most efficient tumor growth suppression effect among all experimental groups and it may be due to the simultaneous delivery of PBA and CUR in NPs (Fig. 8A). As identified in cell-based assays (Figs. 5 and 6), co-treatment of PBA and CUR can amplify their anticancer potentials in A549 tumors. No significant difference among all experimental groups in the body weight implies the absence of severe systemic toxicities after multiple dosing of HAPBA10/CUR NPs (Fig. 8B). Safety of HAPBA10/CUR NPs in heart, liver, lung, kidney, and spleen was also verified by H&E staining (Fig. 8C). Although HAPBA10/CUR NPs were distributed in non-target organs, they did not induce obvious pathophysiological alterations in those organs. On the while, apoptosis induction was clearly observed in HAPBA10/CUR NPs group compared with the other groups. Along with the data of TUNEL assay, relative expression levels of caspase-3 and c-PARP were higher in HAPBA10/CUR NPs group rather than the other groups (Fig. 8D). Anticancer potentials of PBA (*i.e.,* cell cycle arrest, antiproliferation, and apoptosis) seem to be exerted with CUR after intravenous injection in A549 tumor-bearing mouse model. It is worth noting that PBA-installed NPs can enhance the anticancer activities of CUR without severe systemic toxicities.

Conclusions

Short chain fatty acid-grafted HA, acting as an HDAC inhibiting HA derivative, was synthesized and used for the preparation of NPs aiming at tumor-targeted delivery of CUR to lung adenocarcinoma. The roles of PBA were assigned as a hydrophobic segment for nanoassembly structure and an HDAC inhibitor for cancer therapy. PBA can be released from

View Article Online
DOI: 10.1039/C9BM00895K

HAPBA10 *via* an esterase-sensitive cleavage of ester bond after its endocytosis in cancer cells and it may lead to subsequent CUR release. Incorporation of PBA in NPs seemed to enhance the anticancer potentials of CUR in lung adenocarcinoma in this study. CUR and PBA included in NPs improved apoptosis-related anticancer potentials in A549 tumor-bearing mouse models after intravenous injection. Developed HAPBA-based NP may serve as an anticancer potential-boosting nanocarrier with tumor selectivity in cancer therapy.

Conflicts of interest

There are no conflicts to declare.

Acknowledgements

This research was supported by Basic Science Research Program through the National Research Foundation of Korea (NRF) funded by the Ministry of Science, ICT and Future Planning and the Ministry of Education (No. NRF-2017R1E1A1A01074584, NRF-2018R1A6A1A03025582, NRF-2017R1A6A3A11031757, NRF-2017M3A9C8060387, and NRF-2017M3A9C8060390).

References

1 H. S. Hwang, H. Shin, J. Han and K. Na, *J. Pharm. Investig.*, 2018, **48**, 143–151.

2 S. L. Kuan, S. Fischer, S. Hafner, T, Wang, T. Syrovets, W. Liu, Y. Tokura, D. Y. W. Ng, A. Riegger, C. Förtsch, D. Jäger, T. F. E. Barth, T. Simmet, H. Barth and T. Weil, *Adv. Sci.*, 2018, **5**, 1701036.

3 T. Sim, C. Lim, N. H. Hoang and K. T. Oh, *J. Pharm. Investig.*, 2017, **47**, 383–394.

4 D. Yu, O. F. Khan, M. L. Suvà, B. Dong, W. K. Panek, T. Xiao, M. Wu, Y. Han, A. U.

View Article Online
DOI: 10.1039/C9BM00895K

Ahmed, I. V. Balyasnikova, H. F. Zhang, C. Sun, R. Langer, D. G. Anderson and M. S. Lesniak, *Proc. Natl. Acad. Sci. U. S. A.*, 2017, **114**, E6147–E6156.

5 J. Fang, H. Nakamura and H. Maeda, *Adv. Drug Deliv. Rev.*, 2011, **63**, 136–151.

6 F. Danhier, O. Feron and V. Préat, *J. Control. Release*, 2010, **148**, 135–146.

7 C.H. Kim, S.G. Lee, M.J. Kang, S. Lee and Y.W. Choi, *J. Pharm. Investig.*, 2017, **47**, 203–227.

8 B.P. Toole, *Nat. Rev. Cancer*, 2004, **4**, 528–539.

9 F. Dosio, S. Arpicco, B. Stella and E. Fattal, *Adv. Drug Deliv. Rev.*, 2016, **97**, 204–236.

10 U. Günthert, M. Hofmann, W. Rudy, S. Reber, M. Zöller, I. Haußmann, S. Matzku, A. Wenzel, H. Ponta and P. Herrlich, *Cell*, 1991, **65**, 13–24.

11 G. Tripodo, A. Trapani, M. L. Torre, G. Giammona, G. Trapani and D. Mandracchia, *Eur. J. Pharm. Biopharm.*, 2015, **97**, 400–416.

12 B. Yang, B. L. Yang, R. C. Savani and E. A. Turley, *EMBO J.*, 1994, **13**, 286–296.

13 J. H. Park, H. J. Cho, H. Y. Yoon, I. S. Yoon, S. H. Ko, J. S. Shim, J. H. Cho, J. H. Park, K. Kim, I. C. Kwon and D. D. Kim, *J. Control. Release*, 2014, **174**, 98–108.

14 H. J. Cho, H. Y. Yoon, H. Koo, S. H. Ko, J. S. Shim, J. H. Lee, K. Kim, I. C. Kwon and D. D. Kim, *Biomaterials*, 2011, **32**, 7181–7190.

15 H. J. Cho, I. S. Yoon, H. Y. Yoon, H. Koo, Y. J. Jin, S. H. Ko, J. S. Shim, K. Kim, I. C. Kwon and D. D. Kim, *Biomaterials*, 2012, **33**, 1190–1200.

16 J.Y. Jeong, E.H. Hong, S.Y. Lee, J.Y. Lee, J.H. Song, S.H. Ko, J.S. Shim, S. Choe, D.D. Kim, H.J. Ko and H.J. Cho, *Acta. Biomater.*, 2017, **53**, 414–426.

17 Y. J. Jin, U. Termsarasab, S. H. Ko, J. S. Shim, S. Chong, S. J. Chung, C. K. Shim, H. J. Cho and D. D. Kim, *Pharm. Res.*, 2012, **29**, 3443–3454.

18 J. Y. Lee, U. Termsarasab, J. H. Park, S. Y. Lee, S. H. Ko, J. S. Shim, S. J. Chung, H. J. Cho and D. D. Kim, *J. Control. Release*, 2016, **236**, 38–46.

View Article Online
DOI: 10.1039/C9BM00895K

19 S. Y. Lee, J. H. Park, S. H. Ko, J. S. Shim, D. D. Kim and H. J. Cho, *ACS Appl. Mater. Interfaces*, 2017, **9**, 22308–22320.

20 A. Mero and M. Campisi, *Polymers*, 2014, **6**, 346–369.

21 C. E. Schanté, G. Zuber, C. Herlin and T. F. Vandamme, *Carbohydr. Polym.*, 2011, **85**, 469–489.

22 M. Kusaczuk, M. Bartoszewicz and M. Cechowska-Pasko, *Curr. Pharm. Des.*, 2015, **21**, 2147–2166.

23 T. Iannitti and B. Palmieri, *Drugs R. D.*, 2011, **11**, 227–249.

24 B. Lee, W. Rhead, G. A. Diaz, B. F. Scharschmidt, A. Mian, O. Shchelochkov, J. F. Marier, M. Beliveau, J. Mauney, K. Dickinson, A. Martinez, S. Gargosky, M. Mokhtarani and S. A. Berry, *Mol. Genet. Metab.*, 2010, **100**, 221–228.

25 M. A. Carducci, J. Gilbert, M. K. Bowling, D. Noe, M. A. Eisenberger, V. Sinibaldi, Y. Zabelina, T. L. Chen, L. B. Grochow and R. C. Donehower, *Clin. Cancer Res.*, 2001, **7**, 3047–3055.

26 H. H. Engelhard, R. J. Homer, H. A. Duncan and J. Rozental, *J. Neurooncol.*, 1998, **37**, 97–108.

27 M. A. Lea, M. Sura and C. Desbordes, *Anticancer Res.*, 2004, **24**, 2765–2771.

28 I. Svechnikova, S. G. Gray, J. Kundrotiene, F. Ponthan, P. Kogner and T. J. Ekström, *Int. J. Oncol.*, 2003, **22**, 579–588.

29 A. Matelová, G. Huerta-Angeles, D. Šmejkalová, Z. Brůnová, J. Dušek, R. Vícha and V. Velebný, *Carbohydr. Polym.*, 2016, **151**, 1175–1183.

30 S. Y. Lee and H. J. Cho, *Biomacromolecules*, 2019, **20**, 835–845.

31 S. Y. Lee and H. J. Cho, *Drug Deliv.*, 2018, **25**, 738–749.

32 J. J. Lee, S. Y. Lee, J. H. Park, D. D. Kim and H. J. Cho, *Int. J. Pharm.*, 2016, **509**, 483–491.

View Article Online
DOI: 10.1039/C9BM00895K

33 J. Y. Lee, S. J. Chung, H. J. Cho and D. D. Kim, *Adv. Funct. Mater.*, 2015, **25**, 3705–3717.

34 S. Y. Lee, S. H. Ko, J. S. Shim, D. D. Kim and H. J. Cho, *ACS Appl. Mater. Interfaces*, 2018, **10**, 36628–36640.

35 G. Leone, M. Consumi, S. Lamponi and A. Magnani, *Carbohydr. Polym.*, 2012, **88**, 799–808.

36 M. H. Abu Elella, R. R. Mohamed and M. W. Sabaa, *Carbohydr. Polym.*, 2018, **189**, 107–114.

37 L. Cortez and V. Sim, *Prion*, 2014, **8**, 197–202.

38 R. Berni Canani, M. Di Costanzo, L. Leone, M. Pedata, R. Meli and A. Calignano, *World J. Gastroenterol.*, 2011, **17**, 1519–1528.

39 X. Wang, X. Wei, Q. Pang and F. Yi, *Acta Pharm. Sin. B*, 2012, **2**, 387–395.

40 Y. Su, Y. Liu, X. Xu, J. Zhou, L. Xu, X. Xu, D. Wang, M. Li, K. Chen and W. Wang, *ACS Appl. Mater. Interfaces*, 2018, **10**, 38700–38714.

41 S. H. Hong, K. Larocque, D. B. Jaunky, A. Piekny and J. K. Oh, *Colloids Surf. B Biointerfaces*, 2018, **172**, 608–617.

42 Y. H. Choi and H. K. Han, *J. Pharm. Investig.*, 2018, **48**, 43–60.

43 M. J. Ernsting, M. Murakami, A. Roy and S. D. Li, *J. Control. Release*, 2013, **172**, 782–794.

44 R. Aluri, S. Saxena, D. C. Joshi and M. Jayakannan, *Biomacromolecules*, 2018, **19**, 2166–2181.

45 N. G. Vallianou, A. Evangelopoulos, N. Schizas and C. Kazazis, *Anticancer Res.*, 2015, **35**, 645–651.

46 A. A. Lane and B. A. Chabner, *J. Clin. Oncol.*, 2009, **27**, 5459–5468.

View Article Online
DOI: 10.1039/C9BM00895K

Table 1

Particle characterization of developed NPs.

Group	Mean diameter (nm)	Polydispersity index	Zeta potential (mV)	Encapsulation efficiency (%)	Loading amount (%)
HAPBA02 NPs	900 ± 53	0.51 ± 0.03	-21.03 ± 2.12	-	
HAPBA05 NPs	977 ± 182	0.56 ± 0.10	-26.70 ± 0.67	-	
HAPBA10 NPs	721 ± 156	0.37 ± 0.10	-22.70 ± 0.30	-	
HAPBA02 /CUR NPs	597 ± 13	0.14 ± 0.01	-22.95 ± 2.21	52.6 ± 1.3	3.39 ± 0.08
HAPBA05 /CUR NPs	549 ± 13	0.12 ± 0.02	-24.19 ± 1.69	55.4 ± 0.6	3.56 ± 0.03
HAPBA10 /CUR NPs	265 ± 5	0.19 ± 0.02	-24.75 ± 0.52	53.5 ± 0.1	3.45 ± 0.01

Data are presented as the mean ± standard deviation (SD) (n = 3).

$$\text{Encapsulation efficiency } (\%) = \frac{\text{actual amount of drug in NPs}}{\text{input amount of drug in NPs}} \times 100$$

$$\text{Loading amount } (\%) = \frac{\text{actual amount of drug in NPs}}{\text{total amount of drug} - \text{loaded NPs}} \times 100$$

View Article Online
DOI: 10.1039/C9BM00895K

Figure legends

Fig. 1. Scheme of anticancer potentials of developed CUR-loaded HAPBA NPs.

Fig. 2. Synthesis of HAPBA derivatives and their identification. (A) Synthetic sketch of HAPBA. (B) ^{1}H-NMR spectra of HAPBA02, HAPBA05, and HAPBA10. Chemical shifts at 1.8-1.9 ppm (peak 1) and 7.1-7.3 ppm (peak 2 and 3) indicate HA and PBA, respectively. All HAPBA derivatives were dissolved in the mixture of D_2O and DMSO-d_6 (1:1, v/v) for ^{1}H-NMR analysis. (C) Incubation time-dependent PBA release profile from HAPBA10. Released amounts (%) of PBA in the presence or absence of esterase with HAPBA10 are shown. Each point represents the mean ± SD (n = 3).

Fig. 3. Particle characteristics of HAPBA10/CUR NPs. (A) Particle size distribution diagram of HAPBA10/CUR NPs. (B) Particle morphology of HAPBA10/CUR NPs observed by TEM imaging. The length of scale bar in the image is 200 nm. (C) Particle stability of HAPBA10/CUR NPs after incubation in PBS (pH 7.4). Incubation time-dependent hydrodynamic size values are plotted. Each point represents the mean ± SD (n = 3). (D) CUR release profile of HAPBA10/CUR NPs at pH 7.4 and 5.5. Each point represents the mean ± SD (n = 3).

Fig. 4. Cellular accumulation and localization studies of Cy5.5-tagged NPs in A549 cells. (A) Cellular internalization efficiency of fabricated NPs measured by flow cytometry. Cy5.5 and Cy5.5-HAPBA10/CUR NPs were incubated for 1, 2, and 6 h. Each point represents the mean ± SD (n = 3). $^{\#}p < 0.05$, compared with Cy5.5 group. (B) Cellular localization of prepared NPs monitored by CLSM imaging. Cy5.5 and Cy5.5-HAPBA10/CUR NPs were incubated

View Article Online
DOI: 10.1039/C9BM00895K

for 1, 2, and 6 h. Red and blue indicate Cy5.5 and DAPI, respectively. The length of the scale bar in the image is 20 μm.

Fig. 5. *In vitro* antiproliferation potential tests in A549 cells. (A) PBA concentration-dependent cytotoxicity test. PBA or PBA + CUR (10 μg/mL) was applied to the cells. Each point represents the mean ± SD (n = 3). $^{\perp}p < 0.05$, compared with PBA group. (B) HAPBA10 concentration-dependent cytotoxicity test. HA, HAPBA10, or HAPBA10 + CUR (10 μg/mL) was applied to the cells. Each point represents the mean ± SD (n = 3). $^{\$}p < 0.05$, compared with HA group. $^{\&}p < 0.05$, compared with HAPBA10 group. (C) Cytotoxicity test of HAPBA10/CUR NPs. CUR concentration-dependent cell viability value is presented. Each point represents the mean ± SD (n = 3). $^{+}p < 0.05$, compared with CUR group. $^{/}p < 0.05$, compared with HAPBA10 + CUR group.

Fig. 6. Apoptosis assay of CUR-loaded NPs in A549 cells. Annexin V-FITC and PI-based assay was used for assessing the apoptosis inducing effects of HAPBA10, CUR, HAPBA10/CUR NPs, PBA, and PBA + CUR groups after incubation for 24 and 48 h. Population percentage of each panel is presented. UL, UR, LL, and LR indicate upper left, upper right, lower left, and lower right, respectively.

Fig. 7. NIRF imaging test of developed NPs in A549 tumor-bearing mouse model. Cy5.5 or Cy5.5-HAPBA10/CUR NPs were intravenously injected to the mouse model. (A) Whole body NIRF images at 0 (pre), 4, and 24 h postinjection. Yellow dashed circle indicates the tumor region. (B) Intensity of ROI, presented as effective mean intensity × effective area, profiles in tumor region of Cy5.5 and Cy5.5-HAPBA10/CUR NPs-injection groups. Each point represents the mean ± SD (n = 3). $^{\#}p < 0.05$, compared to Cy5.5 group. (C) *Ex vivo*

View Article Online
DOI: 10.1039/C9BM00895K

NIRF image of Cy5.5 and Cy5.5-HAPBA10/CUR NPs-injection groups at 24 h postinjection. (D) Intensity of ROI values in excised heart, lungs, liver, spleen, kidneys, and tumor at 24 h postinjection. Each point represents the mean ± SD (n = 3). $^{\#}p < 0.05$, compared to Cy5.5 group.

Fig. 8. *In vivo* anticancer activity tests of CUR-entrapped NPs in A549 tumor-bearing mouse models. (A) Time-dependent tumor growth profiles of control, HAPBA10, CUR, and HAPBA10/CUR NPs-injection groups. Error bars of control, HAPBA10, and CUR groups are presented in above-direction, while that of HAPBA10/CUR NPs group is shown in below-direction. Each point indicates the mean ± SD (n = 5–6). $^{*}p < 0.05$, compared with control group. $^{\&}p < 0.05$, compared with HAPBA10 group. $^{+}p < 0.05$, compared with CUR group. (B) Body weight of control, HAPBA10, CUR, and HAPBA10/CUR NPs-injected groups. Each point indicates the mean ± SD (n = 5–6). (C) Images of H&E (heart, liver, lung, kidney, spleen, and tumor) and TUNEL (tumor) staining assays. (D) Relative expression levels of caspase-3 and c-PARP (compared to β-actin), measured by western blotting assay, in excised tumor tissues. $^{*}p < 0.05$, compared with control group. $^{\&}p < 0.05$, compared with HAPBA10 group. $^{+}p < 0.05$, compared with CUR group.

View Article Online
DOI: 10.1039/C9BM00895K

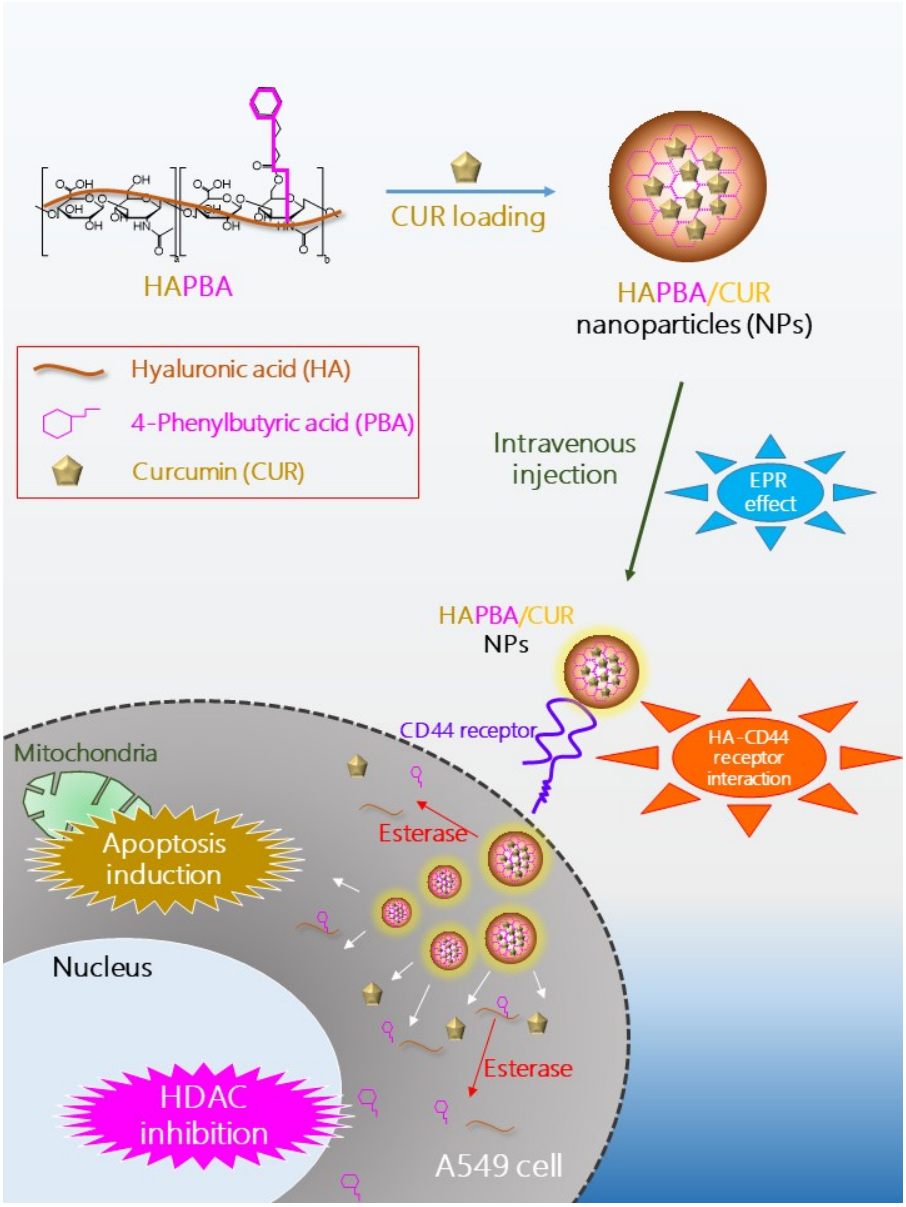

Figure 1

190x254mm (96 x 96 DPI)

View Article Online
DOI: 10.1039/C9BM00895K

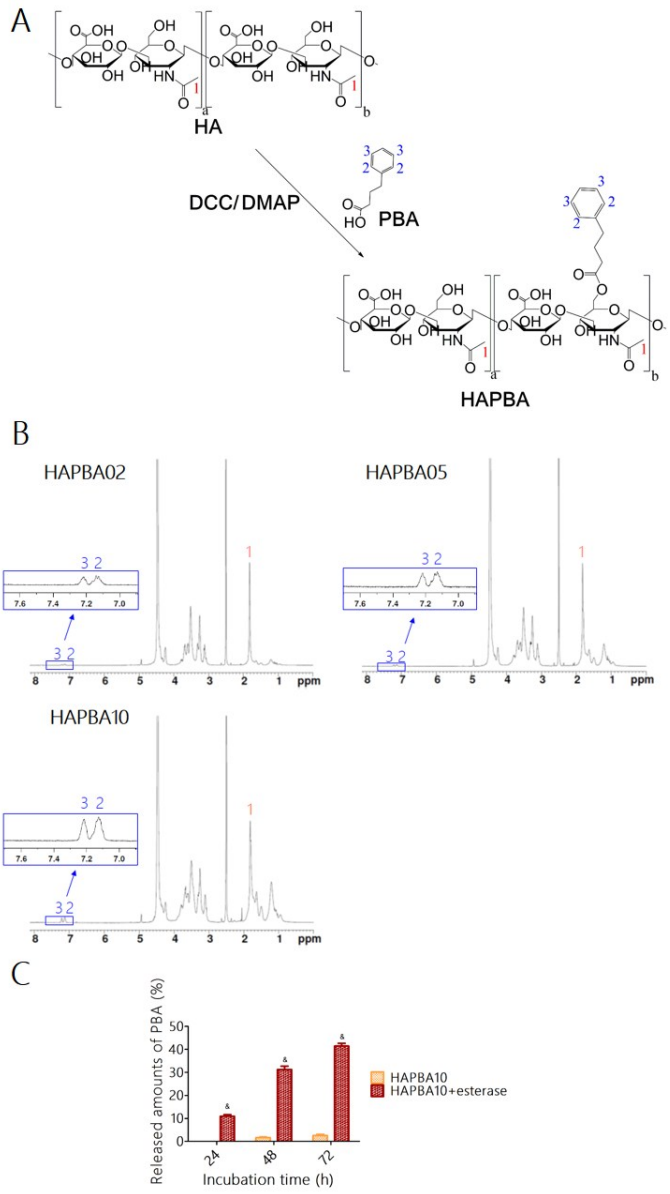

Fig. 2

190x338mm (96 x 96 DPI)

View Article Online
DOI: 10.1039/C9BM00895K

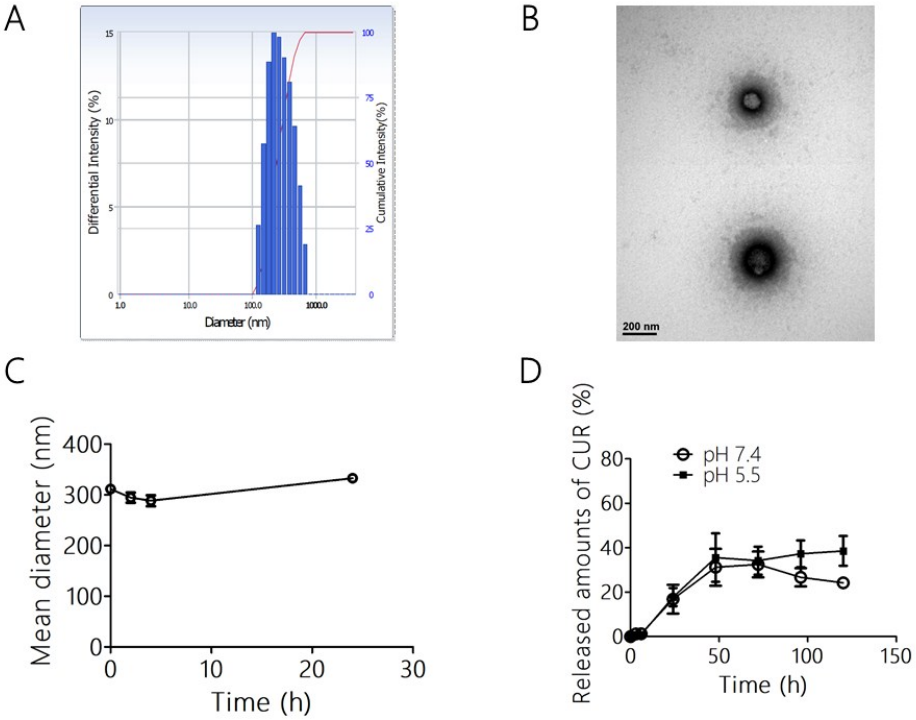

Fig. 3

254x190mm (96 x 96 DPI)

View Article Online
DOI: 10.1039/C9BM00895K

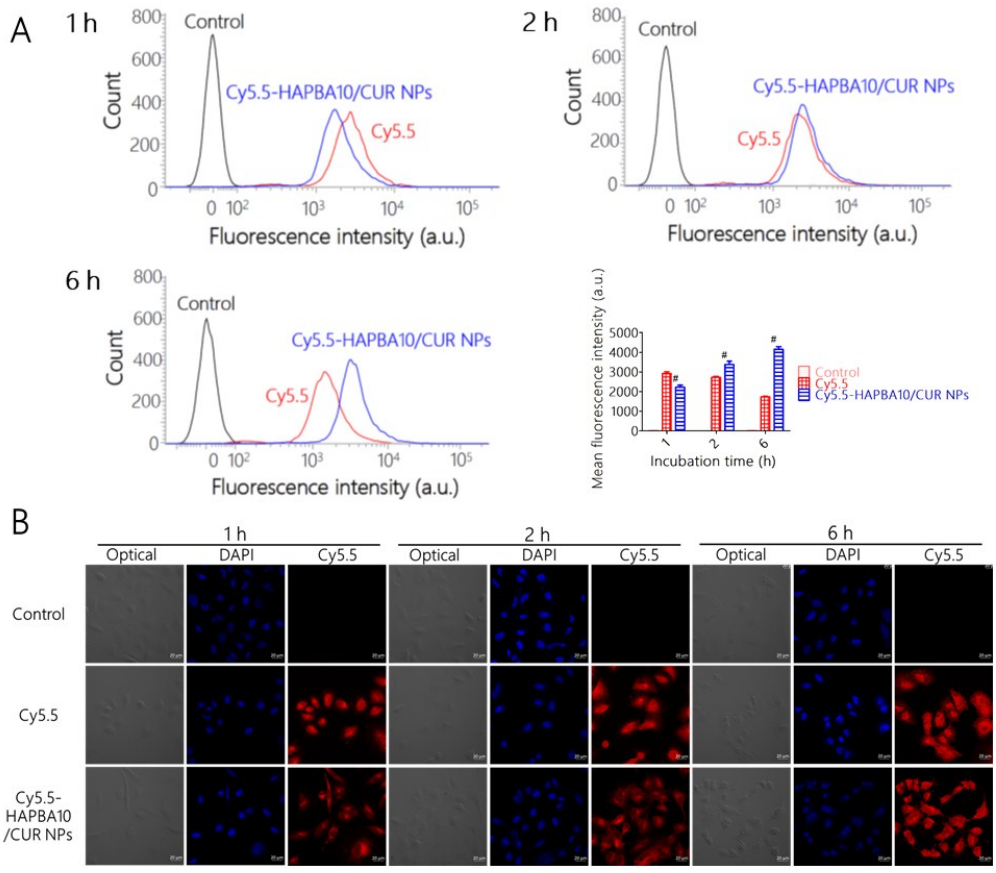

Fig. 4

254x220mm (96 x 96 DPI)

View Article Online
DOI: 10.1039/C9BM00895K

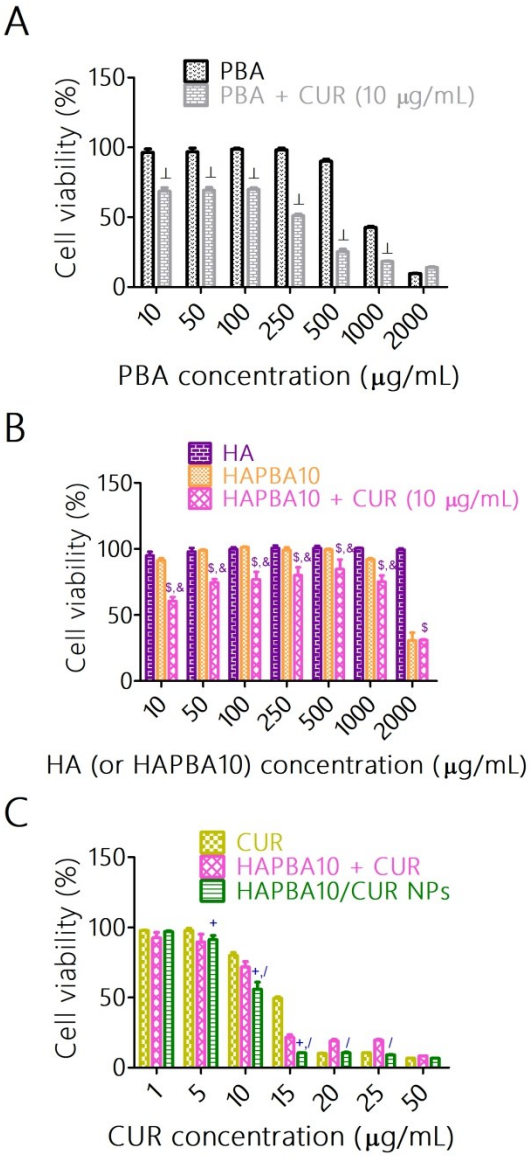

Figure 5

134x282mm (300 x 300 DPI)

View Article Online
DOI: 10.1039/C9BM00895K

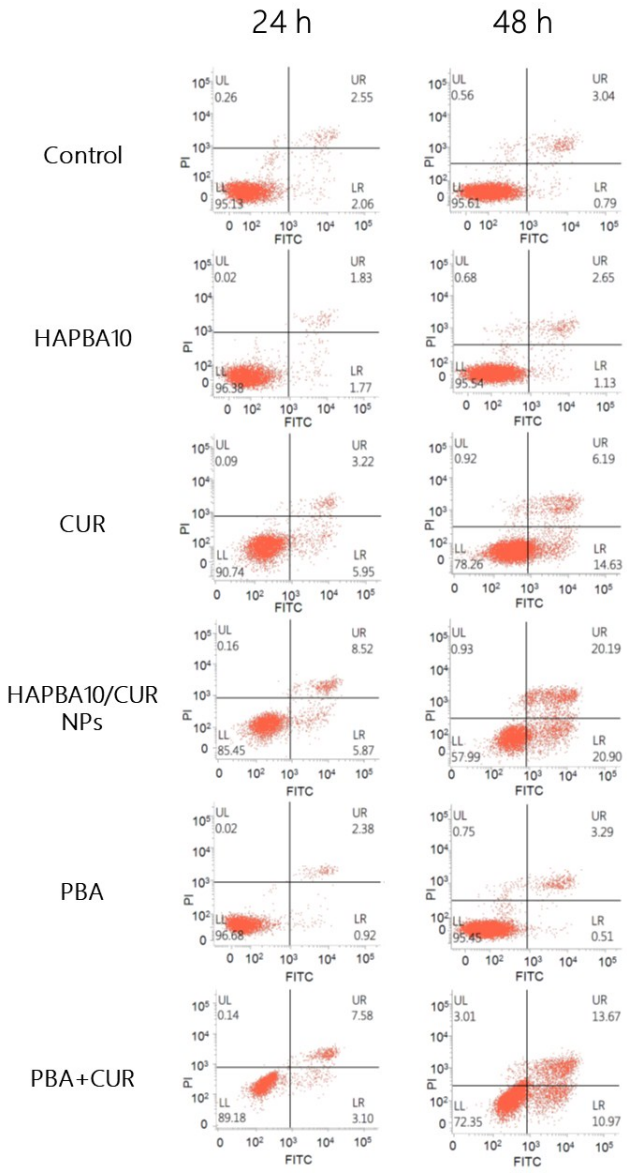

Fig. 6

190x338mm (96 x 96 DPI)

View Article Online
DOI: 10.1039/C9BM00895K

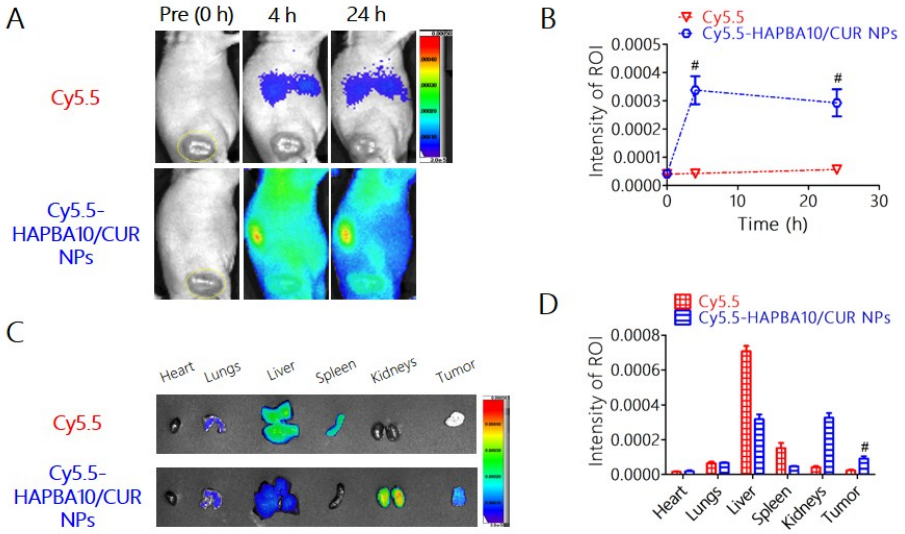

Fig. 7

254x142mm (96 x 96 DPI)

View Article Online
DOI: 10.1039/C9BM00895K

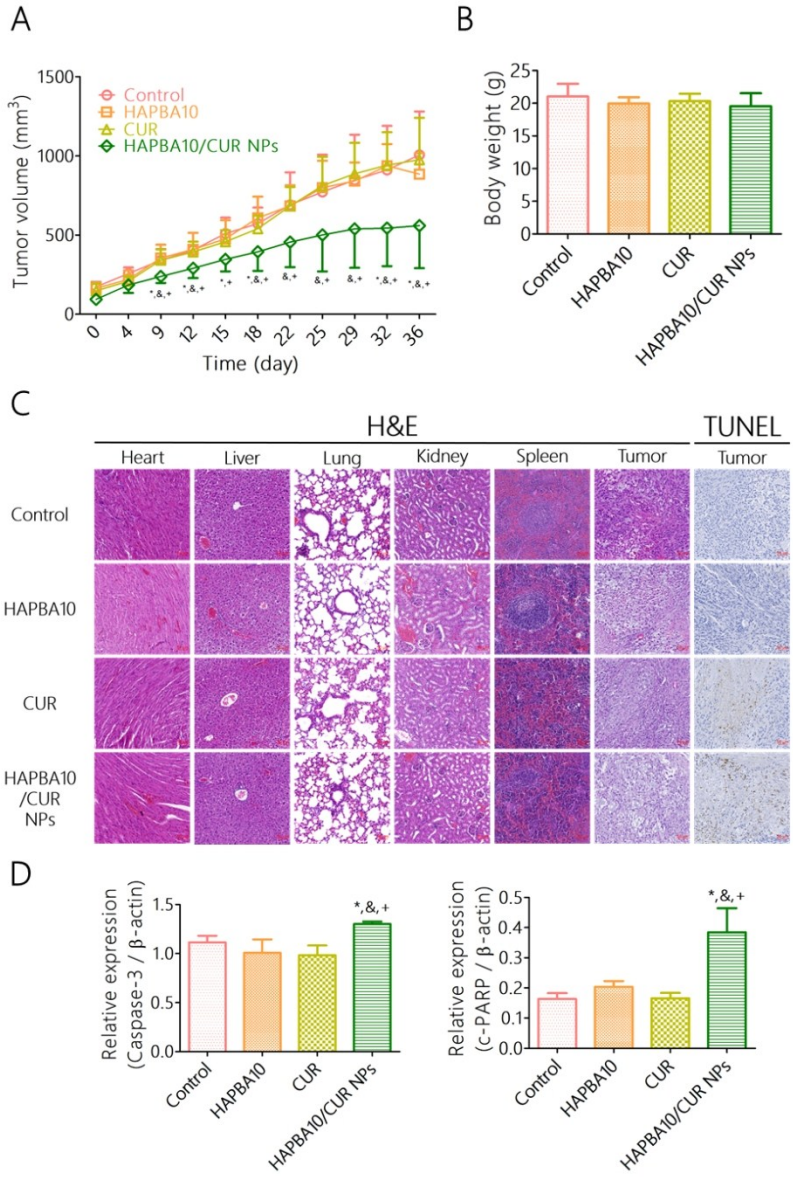

Figure 8

250x370mm (96 x 96 DPI)